Independent Flexural Wave Frequency Conversion by a Linear Active Metalayer

Qian Wu,[1] Xiaodong Zhang,[2] P. Shivashankar,[1] Yangyang Chen,[3,*] and Guoliang Huang [1,†]

[1]*Department of Mechanical and Aerospace Engineering, University of Missouri, Columbia, Missouri 65211, USA*
[2]*College of Mechanical Engineering and Automation, Huaqiao University, 361021 Xiamen, China*
[3]*Department of Mechanical and Aerospace Engineering, The Hong Kong University of Science and Technology,
Clear Water Bay, 999077 Hong Kong, China*

Wave frequency is a critical parameter for applications ranging from structural health monitoring, noise control, and medical imaging to quantum of energy in matter. Frequency conversion is an inevitable wave phenomenon in nonlinear or time-modulated media. However, frequency conversion in linear media holds the promise of breaking limits imposed by the physics laws of wave diffraction such as Snell's law and Rayleigh criterion. In this Letter, we physically introduce a linear active metalayer in a structural beam that can convert the wave frequency of an flexural incidence into arbitrary frequencies of transmitted waves, which is underpinned by time modulation of sensing signals and insensitive to incident amplitude. The active element, involving piezoelectric components and time-modulated transfer function, breaks energy conservation such that the generated harmonics can be fully decoupled, making the frequency conversion linear and independent. By leveraging the time-modulated unit, phase-gradient and frequency-gradient metalayers are proposed for frequency-converted wave steering and dynamic beam steering, respectively. The linear active metalayer proposed herein suggests a promising solution to fully control time-domain signals of flexural waves, in stark contrast with existing elastic metasurfaces, regardless of being passive or active.

Wave frequency is one of the fundamental parameters governing wave propagation and its interaction with matters. Most physical laws on wave propagation and wave-matter interaction are frequency-dependent. Altering frequency can break the limits currently imposed by laws of physics for a given frequency condition, such as imaging resolution limits, wave energy transport, and wave propagation behavior. Manipulating flexural waves in platelike structures has been of considerable interest with widespread applications in nondestructive structural health monitoring, vibration suppression and control [1–8]. In linear time-invariant plate-type media, energy exchange among waves at different frequencies is prohibited since those waves are decoupled. On the other hand, flexural waves at different frequencies can exchange energy among themselves due to the coupling and mixing of different frequency components during the propagation in nonlinear or time-modulated plate media, where linearity or time invariance is broken [9–14]. However, nonlinear and time-modulated wave conversion is in general amplitude-dependent and also takes place in a way that is impossible to be manipulated individually and independently, limiting its wave control applications [12–15]. A linear mechanism-based wave conversion, which is independent of incident amplitude and provides generation of freely controlled harmonics, could offer far more freedom in wave manipulation and therefore is the major motivation of this study.

Rapid advances in control of the phase and amplitude of wave scattering from planar or linear arrays of scatterers have stimulated the development of optic, acoustic, and elastic metasurfaces with subwavelength building blocks that use amplitude or phase-sensitive scattering to enable wavefront control. To date, metasurfaces have mostly been designed for wave beam steering [16–20] and focusing [20–22], self-bending beam generation [20,23], control of dynamic pulse [24,25], as well as wave mode and polarization conversion [26–28]. To enhance their functionality and dynamic performance in scenarios where tunability and adaptivity are required, active metasurfaces have been recently suggested by incorporating an active medium into passive metasurface structure. For example, the active mechanical metalayers have been developed by introducing piezoelectric sensors and actuators into host structures [29,30]. Thus far, the active metasurfaces reported are mainly linear and time-invariant for dynamic control, and the interference wave phenomena are only observed at single frequency. To exploit the frequency mixing, optical time-varying metasurfaces have been proposed [31,32]. In those designs, the refractive index is temporally modulated using a pump or carrier wave, efficiently enabling enriched wave functions compared with time-invariant designs, i.e., simultaneous control of spatial and temporal spectra of light [33,34], and modulated frequency conversion [35]. However, to the best of our knowledge, there exists no
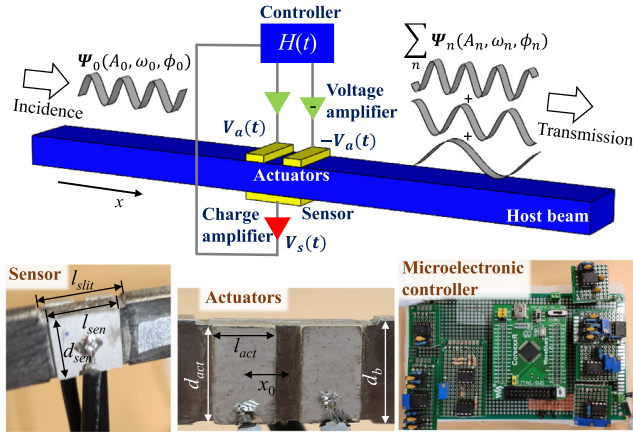
FIG. 1. Schematic illustration of the programmable time-modulated metabeam for continuous dynamic control of flexural wave propagation. The meta cell converts the incident wave $\Psi_0(A_0, \omega_0, \phi_0)$ into an arbitrary combination of transmitted wave components $\Sigma_n \Psi_n(A_n, \omega_n, \phi_n)$, via a programmable feed-forward control system that exhibits time modulation and realizes antisymmetric actuation. The terms A_n, ω_n, and ϕ_n denote the field magnitude, frequency, and phase of the nth-order harmonic, respectively. The bottom layer shows the photos of the mechanical (actuators and sensor) and the microelectronic control circuit. The piezoelectric patches (PZT-5J, $l_{sen} = d_{sen} = d_{act} = 10$ mm, $l_{act} = 4$ mm, $x_0 = 3$ mm) are mounted to a 3-mm-thick steel beam of $d_b = 11$ mm via conductive epoxy. The thicknesses of the sensor and actuators are 0.5 mm and 1 mm, respectively. The slit used to diminish the interactions between adjacent meta cells has a length of $l_{slit} = 12$ mm. The microelectronic controller is responsible for generating the time-dependent transfer function. $V_s(t)$ and $V_a(t)$ are the respective electrical voltages from the charge amplifier and voltage amplifier. They follow the relationship $H(t) = V_a(t)/V_s(t)$.

strategies or designs of linear metasurfaces that could achieve independent and controllable frequency conversion in optics, acoustics, and mechanics.

In this Letter, we report a linear active metalayer in a structural beam for independent frequency conversion of flexural waves, which is underpinned by a unique physical principal related to circuit time modulation of sensing signals. The active metalayer is driven by a time-dependent transfer function through bonded piezoelectric actuators and sensors to perform independent parallel operations over waves at different frequencies. The design breaks energy conservation by pumping in electrical energy to cancel incidence and freely emit arbitrary transmitted waves as demanded (Fig. 1). To the best of our knowledge, no existing experimental designs can break the fundamental limitation imposed by the physics laws of wave diffraction such as Snell's law and Rayleigh criterion to realize such linear and independent mode conversion of flexural waves in a very thin dimension. Additionally, phase- and frequency-gradient metalayers for frequency-converted wave steering and dynamic beam steering are demonstrated,

respectively. The physical realization of the metalayer is the key to accomplish these novel wave functions.

The linear active metalayer is constructed by bonding a large piezoelectric patch on one surface and two small piezoelectric patches on another surface of a host beam (see Fig. 1). The large piezoelectric patch serves as the sensor to sense the bending curvature at its position. The two small piezoelectric patches are actuators that can generate bending moments to the beam. The sensor and actuators are connected by an electrical control loop. In the design, a charge amplifier is connected to the sensing patch, leading to the sensing voltage $V_s(t)$. We apply antisymmetric voltages on the two patches [one is $V_a(t)$, the other is $-V_a(t)$], which collectively produce an effective shear load on the beam. As a result, the sensor cannot detect the actuation, making the control loop feedforward. A digital microcontroller is implemented into the electrical control loop to send out the signal $V_a(t)$ based on the input $V_s(t)$. Remarkably, the feed-forward control loop enables multiple independent parallel operations in the microcontroller, as each of the operations has no effect on the sensing signal, preventing interactions with other operations. To realize frequency conversion, the microcontroller is driven by two independent operations to generate the superimposed actuation signal as $V_a(t) = V_a^{(0)}(t) + \bar{V}_a(t)$, where $V_a^{(0)}(t)$ is used to cancel the incident wave in the transmitted field and $\bar{V}_a(t) = \sum_{n=1}^{N} V_a^{(n)}(t)$ is mainly for the wave conversion with multiple desired frequencies in the transmitted field.

To find the relationship between $V_a^{(0)}(t)$ and $V_s(t)$, we first calculate the wave field generated by $V_a^{(0)}(t)$ using Green's function as

$$\tilde{w}_a(x) = \text{sgn}(x)(e^{-ik_1|x|} + e^{-k_2|x|})\kappa_a\tilde{V}_a, \qquad (1)$$

where $\tilde{w}_a(x)$ and $\tilde{V}_a$ denote the harmonic wave profile and the amplitudes of the actuation voltage, and κ_a, k_1, and k_2 are real constants representing the actuation coefficient, wave number, and attenuation constant, respectively (see Supplemental Material [36] for detailed definition). In the derivation, we assume the active metalayer is located at $x = 0$, and the dimension of the metalayer is much shorter than the wavelength such that the actuation of the metalayer can be treated as a point shear load. Considering an incident flexural wave $\tilde{w}_i(x) = \tilde{W}_i e^{-ik_1 x}$ with a complex amplitude $\tilde{W}_i$, the sensing signal can be obtained as $\tilde{V}_s = \tilde{W}_i/\kappa_s$, where κ_s is a real constant denoting the sensing coefficient. To achieve wave cancellation in the transmitted field, the traveling wave component of $\tilde{w}_a(x)$ should be out of phase with $\tilde{w}_i(x)$ for $x > 0$, leading to

$$\frac{\tilde{V}_a}{\tilde{V}_s} = -\frac{\kappa_s}{\kappa_a}. \qquad (2)$$

As a result, $V_a^{(0)}(t)$ is always proportional to $V_s(t)$. This simple relationship, however, produces complexity to the design of the electrical control system in experiments, as the control system usually requires filters for system stability, which, otherwise, induce the phase change between $V_a^{(0)}(t)$ and $V_s(t)$. In experiment, we employ an analog differentiator circuit together with a second-order filter in the microcontroller to approximate this linear relationship (see Supplemental Material [36] for detailed circuit designs). In particular, the relationship between the output and input signals of the second-order filter in the microcontroller reads $(\ddot{V}_{out}/\omega_0^2) + (\dot{V}_{out}/2\mu\omega_0) + V_{out} = A_0 V_{in}$, where $\mu = 0.6$, $A_0 = (\kappa_s/2\mu\kappa_a)$, and the cutoff frequency ω_0 is selected as the operation frequency.

Next, to construct $V_a^{(n)}(t)$ using $V_s(t)$ for active emission of waves at a different frequency, we consider harmonic incidence with a real time-domain sensing signal $V_s(t) = (\tilde{W}_i/\kappa_s)\cos(\omega t + \phi_0)$. With this assumption, $V_a^{(n)}(t)$ can be attained by mixing $V_s(t)$ with a carrier wave as

$$V_a^{(n)}(t) = A_n\left[V_s(t)\cos(\delta\omega_n t + \phi_n)\right.$$
$$\left. - V_s\left(t - \frac{3\pi}{2\omega}\right)\sin\left(\delta\omega_n t + \phi_n\right)\right], \quad (3)$$

where A_n controls the amplitude of the emitted wave, $\delta\omega_n$ is the change in frequency, and ϕ_n modulates the phase of the emitted wave. Note that the presence of $V_s[t - (3\pi/2\omega)]$ requires the prior knowledge of the sensing signal. In experiments, instead of recording the sensing signal in the microcontroller, we calculate $\dot{V}_s(t)$ at the current time step, and let $V_s[t - (3\pi/2\omega)] = [\dot{V}_s(t)/\omega]$. Using Eq. (3), $\bar{V}_a(t)$ can be electronically computed in parallel with $V_a^{(0)}(t)$, and the total excitation voltage $V_a(t)$ is enabled for frequency conversion. Note that the active metalayer for frequency conversion is designed at a single frequency, which should also be known before its operation. However, in practical applications, adaptive filters can be implemented into the microcontroller, which could circumvent the need of the prior knowledge of the operation frequency. In addition, the active metalayer can work well for narrow-band signals, not just single-frequency incidences, evidenced by the results reported below.

To validate the design for frequency conversion, we fabricate the linear active metalayer on a steel beam and construct the corresponding electrical control system for experimental testing (see Supplemental Material [36] for details). In experiments, incident flexural waves are launched from the left of the active metalayer using a piezoelectric actuator bonded on the host beam. We select 15-peak tone-burst signals with the central frequency being 10 kHz as incident signals. The out-of-plane velocity field
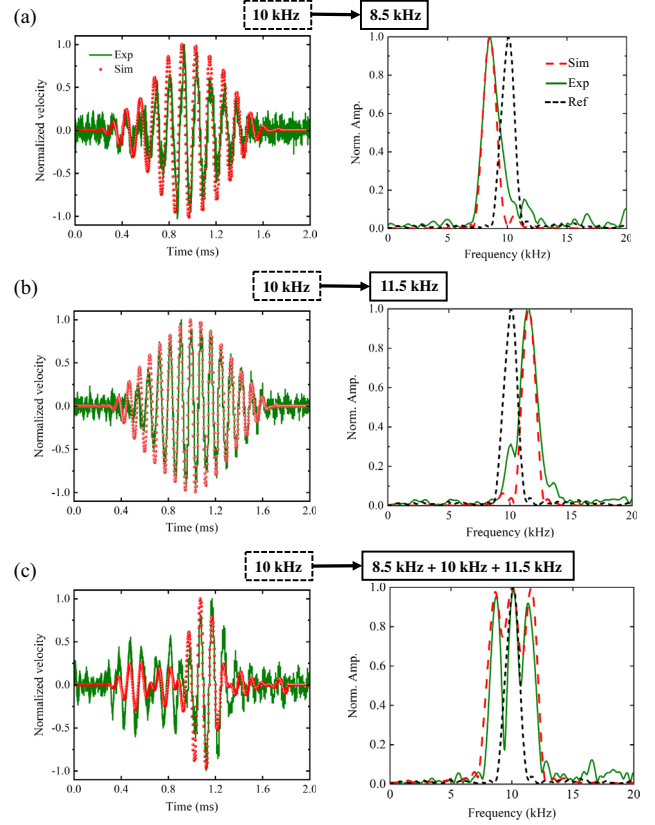

FIG. 2. Demonstrations of the frequency shifting function in three typical scenarios: 10 kHz incidence is converted into (a) transmission of 8.5 kHz, (b) transmission of 11.5 kHz, and (c) transmission of $8.5 + 10 + 11.5$ kHz (frequency comb). The red and green curves represent the numerical and experimental results, respectively. The black dotted curves in the frequency spectra denote the incidence wave as the reference.

in the transmitted domain is measured using a scanning laser Doppler vibrometer. Figure 2 shows the transmitted wave signals in time and frequency domains measured from experiments (green solid curves). For comparison, corresponding time-dependent numerical simulations are performed using COMSOL MULTIPHYSICS (red dashed curves). In Fig. 2(a), frequency down conversion is realized by imposing $N = 1$, $\delta\omega_1 = -2\pi \times 1.5$ kHz, and $\phi_1 = 0$. The black dotted curve in the frequency domain represents the frequency components of the incident wave measured without the electrical control system. It can be clearly seen that the active metalayer successfully converts the frequency from 10 to 8.5 kHz as desired, both experimentally and numerically. Importantly, no waves at other frequencies appear in the transmitted spectrum, in stark contrast with nonlinear and time-modulated materials. Similarly, the linear active metalayer also supports frequency up conversion, i.e., from 10 to 11.5 kHz, by enforcing $\delta\omega_1 = 2\pi \times 1.5$ kHz, as shown in Fig. 2(b). Note that small spectral discrepancies are visible between the experiments and simulations. This could result from the boundary
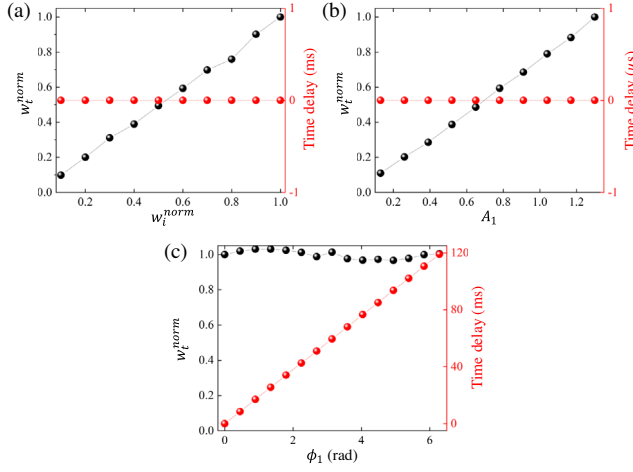
FIG. 3. Linear independent control over frequency conversion from 10 to 8.5 kHz. Transmitted displacement ratio of wave packets w_t^{norm} and time delay are numerically demonstrated by sweeping (a) maximum incident displacement w_i^{norm} from 0.1 to 1, (b) amplitude A_1 given in Eq. (3) from 0.13 to 1.3, and (c) phase shift ϕ_1 from 0 to 2π. In each cases, the parameters that are not swept remain unchanged as used in Fig. 2.

reflection and signal minor distortion in the digital microcontroller, which are not properly considered in the numerical simulation and can result in wider band in the transmitted waves. In addition to the single-frequency conversion, the active metalayer is capable to create frequency-comb signals. To demonstrate this, we let $V_a^{(0)}(t) = 0$, releasing the incident wave to the transmitted domain and impose $N = 2$ with $\delta\omega_1 = -2\pi \times 1.5$ kHz and $\delta\omega_2 = 2\pi \times 1.5$ kHz to actively emit waves with the other two frequency components. As shown in Fig. 2(c), the transmitted wave peaks at three frequencies, 8.5, 10, and 11.5 kHz, as demand. The quality factor of those peaks can be enhanced by impinging incident waves containing enough numbers of peaks in the tone-burst signals.

To illustrate linearity of the active metalayer, we perform numerical simulations with different incidences for the frequency conversion demonstrated in Fig. 2(a). In the simulations, the normalized maximum displacement of the incident wave package, $w_i^{norm} = w_i^{max}/\bar{w}_i^{max}$, changes from 0.1 to 1, where $\bar{w}_i^{max}$ denotes the maximum displacement of the incident wave package with the central frequency being 10 kHz in Fig. 2(a). Figure 3(a) shows the normalized maximum displacement of the transmitted wave package, $w_t^{norm} = w_t^{max}/\bar{w}_t^{max}$, and the relative time delay compared with that in Fig. 2(a). Similarly, $\bar{w}_t^{max}$ represents the maximum displacement of the transmitted wave package with the central frequency being 8.5 kHz in Fig. 2(a). It can be clearly seen that w_t^{norm} is proportional to w_i^{norm}, and the relative time delay remains zero for all w_i^{norm}, indicating linearity of the active metalayer. Further, to show independency between different harmonics of the active metalayer, we conduct another set of numerical simulations
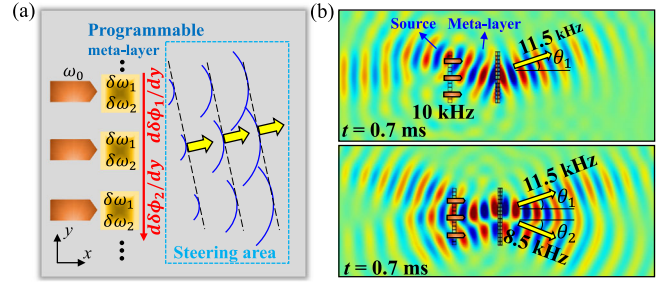

FIG. 4. (a) Schematic of a phase-gradient programmable metalayer that consists of 14 cells and features the flexural beam steering with frequency shifts. The red arrow indicates the phase gradient's direction. (b) Top panel shows flexural beam steering with the frequency shift $\delta\omega = 2\pi \times 1.5$ kHz and phase gradient $d\phi_1/dy = 0.13\pi$ rad/m, while the bottom shows the conversion into additional 8.5 kHz with a phase gradient $d\phi_2/dy = -0.13\pi$ rad/m, respectively. Both fields are obtained at 0.7 ms in the transient analysis. The inputs are set as 10 kHz, and the output wave directions are indicated by the yellow arrows.

with different A_1 and ϕ_1 still for the frequency down conversion demonstrated in Fig. 2(a). As shown in Fig. 3(b), where $\phi_1 = 0$, w_t^{norm} linearly increases with A_1, and the relative time delay still remains close to zero. While, in Fig. 3(c), A_1 keeps unchanged and ϕ_1 increases from 0 to 2π, giving rise to linear changes of the relative time delay. In all the simulations, wave cancellation has not been impaired to any extent, and no waves with other frequency components have been detected in the transmitted domain, successfully demonstrating the independent control over frequency-converted waves.

Implementing an array of the linear active metalayers to a plate enables spacial operations of the wavefront together with the frequency conversion. We first construct a phase-gradient metalayer to steer the frequency-converted wave direction [Fig. 4(a)]. In the simulations, we keep $\delta\omega_1$ and A_1 unchanged among each of the metalayer units and ϕ_1 is arranged to a linear profile along the vertical direction. As shown in the upper panel of Fig. 4(b), the incident wave beam with the central frequency being 10 kHz is transformed to a beam with the central frequency becoming 11.5 kHz and, at the same time, steered to a direction of $\theta_1 = 19.2°$, where $d\phi_1/dy = 0.13\pi$ rad/m. In addition, another frequency-converted wave steering with $\delta\omega_2 = -2\pi \times 1.5$ kHz and $d\phi_2/dy = -0.13\pi$ rad/m is performed. It is noticed that the incident wave beam is transformed into two beams with central frequencies becoming 11.5 and 8.5 kHz, and steered to two directions of 19.2° and −22.4°, respectively [see the lower panel in Fig. 4(b)]. Note that the mixing effect makes the two beams somewhat indistinguishable. This could be resolved by either considering a later time instant or enlarging the frequency difference of the output harmonics.

In addition, we illustrate a frequency-gradient metalayer to realize dynamic wave steering, where the wave in the
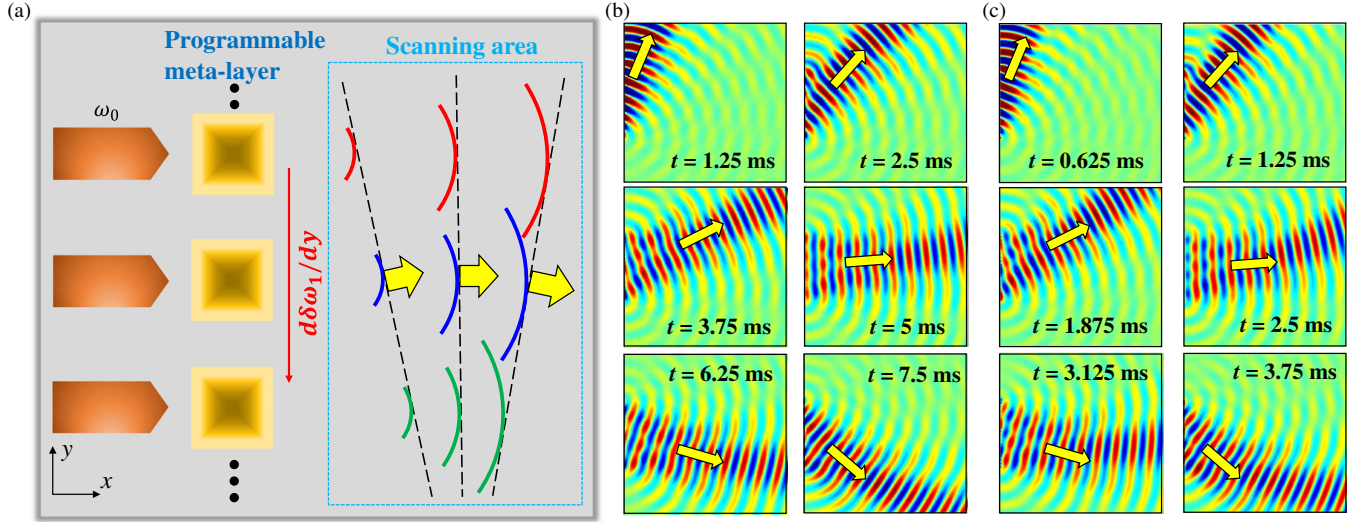
FIG. 5. (a) Schematic of the frequency-gradient programmable metalayer that contains 20 cells and provides dynamic control over the flexural beam steering as time progresses. The red arrow indicates the frequency gradient's direction. (b),(c) Dynamic beam steering over time at the frequency gradients (b) $d\delta\omega_1/dy = 2\pi \times 4.56$ and (c) $2\pi \times 9.12$ kHz/m for 20 metalayer units included. The inputs are set as 10 kHz, and the output wave directions are indicated by the yellow arrows at each time instant.

transmitted domain constantly changes its propagation direction in time [Fig. 5(a)] [34,37]. To construct this metalayer, we keep A_1 and ϕ_1 unchanged among each of the metalayer units and organize a linear profile to $\delta\omega_1$ along the vertical direction. With this, flexural waves coming through each of the metalayer units travel at different frequencies to collectively produce a flexural wave beam rotating in time thanks to the constructive wave interference (see Supplemental Material [36]). Figures 4(b) and 4(c) show the simulated wave fields at different time steps with $d\delta\omega_1/dy = 2\pi \times 4.56$ and $2\pi \times 9.12$ kHz/m. Dynamic wave steering is clearly demonstrated, and a greater $d\delta\omega_1/dy$ induces faster angular speed of the wave beam. Note that we apply continuous sine-wave excitation. Wave dispersion in the free plate can be ignored in this application (see Supplemental Material [36]).

In summary, we introduce a linear active metalayer for independent frequency conversion of flexural waves in elastic beam and plate. The active metalayer is constructed in a beam by mounting piezoelectric elements connected with an electrical controller. The design embraces a feed-forward control loop that can naturally perform time-modulated independent parallel operations. We demonstrate the frequency conversion experimentally and numerically and prove independent wave frequency manipulation ability and its linearity. By implementing the linear active metalayers in a plate, we also show wave beam steering of frequency-converted waves and dynamic beam steering using phase-gradient and frequency-gradient arrangements. Different from existing designs, the linear active metalayer paves a way for fully controlled time-domain signals and wave energy of flexural waves.

Furthermore, thanks to its simplicity, this active design can be easily extended to two- and three-dimensional active metamaterials for even more complicated wave manipulation and control.

Q. W. and X. Z, contributed to this work equally.

*Corresponding author.
maeychen@ust.hk
†Corresponding author.
huangg@missouri.edu

[1] C. H. Wang, J. T. Rose, and F.-K. Chang, A synthetic time-reversal imaging method for structural health monitoring, Smart Mater. Struct. **13**, 415 (2004).

[2] C. R. Farrar and K. Worden, An introduction to structural health monitoring, Phil. Trans. R. Soc. A **365**, 303 (2007).

[3] R. Zhu, X. Liu, G. Hu, C. Sun, and G. Huang, A chiral elastic metamaterial beam for broadband vibration suppression, J. Sound Vib. **333**, 2759 (2014).

[4] H. Peng and P. F. Pai, Acoustic metamaterial plates for elastic wave absorption and structural vibration suppression, Int. J. Mech. Sci. **89**, 350 (2014).

[5] G. Hu, L. Tang, A. Banerjee, and R. Das, Metastructure with piezoelectric element for simultaneous vibration suppression and energy harvesting, J. Vib. Acoust. **139**, 011012 (2017).

[6] H. Peng, P. F. Pai, and H. Deng, Acoustic multi-stopband metamaterial plates design for broadband elastic wave

absorption and vibration suppression, Int. J. Mech. Sci. **103,** 104 (2015).

[7] M. D. Rao, Recent applications of viscoelastic damping for noise control in automobiles and commercial airplanes, J. Sound Vib. **262,** 457 (2003).

[8] Y. Chen, G. Huang, and C. Sun, Band gap control in an active elastic metamaterial with negative capacitance piezoelectric shunting, J. Vib. Acoust. **136,** 061008 (2014).

[9] M. F. Müller, J.-Y. Kim, J. Qu, and L. J. Jacobs, Characteristics of second harmonic generation of lamb waves in nonlinear elastic plates, J. Acoust. Soc. Am. **127,** 2141 (2010).

[10] H. Nassar, B. Yousefzadeh, R. Fleury, M. Ruzzene, A. Alù, C. Daraio, A. N. Norris, G. Huang, and M. R. Haberman, Nonreciprocity in acoustic and elastic materials, Nat. Rev. Mater. **5,** 667 (2020).

[11] H. Nassar, H. Chen, A. Norris, and G. Huang, Nonreciprocal flexural wave propagation in a modulated metabeam, Extreme Mech. Lett. **15,** 97 (2017).

[12] Y. Chen, X. Li, H. Nassar, A. N. Norris, C. Daraio, and G. Huang, Nonreciprocal Wave Propagation in a Continuum-Based Metamaterial with Space-Time Modulated Resonators, Phys. Rev. Applied **11,** 064052 (2019).

[13] G. Trainiti, Y. Xia, J. Marconi, G. Cazzulani, A. Erturk, and M. Ruzzene, Time-Periodic Stiffness Modulation in Elastic Metamaterials for Selective Wave Filtering: Theory and Experiment, Phys. Rev. Lett. **122,** 124301 (2019).

[14] J. Marconi, E. Riva, M. Di Ronco, G. Cazzulani, F. Braghin, and M. Ruzzene, Experimental Observation of Nonreciprocal Band Gaps in a Space-Time-Modulated Beam Using a Shunted Piezoelectric Array, Phys. Rev. Applied **13,** 031001(R) (2020).

[15] X. Xu, Q. Wu, H. Chen, H. Nassar, Y. Chen, A. Norris, M. R. Haberman, and G. Huang, Physical Observation of a Robust Acoustic Pumping in Waveguides with Dynamic Boundary, Phys. Rev. Lett. **125,** 253901 (2020).

[16] M. Zheng, C. I. Park, X. Liu, R. Zhu, G. Hu, and Y. Y. Kim, Non-resonant metasurface for broadband elastic wave mode splitting, Appl. Phys. Lett. **116,** 171903 (2020).

[17] H. Lee, J. K. Lee, H. M. Seung, and Y. Y. Kim, Mass-stiffness substructuring of an elastic metasurface for full transmission beam steering, J. Mech. Phys. Solids **112,** 577 (2018).

[18] B. Assouar, B. Liang, Y. Wu, Y. Li, J.-C. Cheng, and Y. Jing, Acoustic metasurfaces, Nat. Rev. Mater. **3,** 460 (2018).

[19] L. Cao, Z. Yang, Y. Xu, S.-W. Fan, Y. Zhu, Z. Chen, B. Vincent, and B. Assouar, Disordered Elastic Metasurfaces, Phys. Rev. Applied **13,** 014054 (2020).

[20] H. Zhu and F. Semperlotti, Anomalous Refraction of Acoustic Guided Waves in Solids with Geometrically Tapered Metasurfaces, Phys. Rev. Lett. **117,** 034302 (2016).

[21] Y. Jin, W. Wang, A. Khelif, and B. Djafari-Rouhani, Elastic Metasurfaces for Deep and Robust Subwavelength Focusing and Imaging, Phys. Rev. Applied **15,** 024005 (2021).

[22] J. Rong, W. Ye, S. Zhang, and Y. Liu, Frequency-coded passive multifunctional elastic metasurfaces, Adv. Funct. Mater. **30,** 2005285 (2020).

[23] S. Tol, Y. Xia, M. Ruzzene, and A. Erturk, Self-bending elastic waves and obstacle circumventing in wireless power transfer, Appl. Phys. Lett. **110,** 163505 (2017).

[24] M. Dubois, E. Bossy, S. Enoch, S. Guenneau, G. Lerosey, and P. Sebbah, Time-Driven Superoscillations with Negative Refraction, Phys. Rev. Lett. **114,** 013902 (2015).

[25] K. Tang, C. Xu, S. Guenneau, and P. Sebbah, Pulse dynamics of flexural waves in transformed plates, Adv. Funct. Mater. **31,** 2009266 (2021).

[26] M. S. Kim, W. R. Lee, Y. Y. Kim, and J. H. Oh, Transmodal elastic metasurface for broad angle total mode conversion, Appl. Phys. Lett. **112,** 241905 (2018).

[27] X. Su, Z. Lu, and A. N. Norris, Elastic metasurfaces for splitting sv-and p-waves in elastic solids, J. Appl. Phys. **123,** 091701 (2018).

[28] A. Colombi, V. Ageeva, R. J. Smith, A. Clare, R. Patel, M. Clark, D. Colquitt, P. Roux, S. Guenneau, and R. V. Craster, Enhanced sensing and conversion of ultrasonic rayleigh waves by elastic metasurfaces, Sci. Rep. **7,** 6750 (2017).

[29] Y. Chen, X. Li, G. Hu, M. R. Haberman, and G. Huang, An active mechanical willis meta-layer with asymmetric polarizabilities, Nat. Commun. **11,** 1 (2020).

[30] Y. Chen, X. Li, H. Nassar, G. Hu, and G. Huang, A programmable metasurface for real time control of broadband elastic rays, Smart Mater. Struct. **27,** 115011 (2018).

[31] A. Shaltout, A. Kildishev, and V. Shalaev, Time-varying metasurfaces and lorentz non-reciprocity, Opt. Mater. Express **5,** 2459 (2015).

[32] L. Zhang, X. Q. Chen, R. W. Shao, J. Y. Dai, Q. Cheng, G. Castaldi, V. Galdi, and T. J. Cui, Breaking reciprocity with space-time-coding digital metasurfaces, Adv. Mater. **31,** 1904069 (2019).

[33] N. Chamanara, Y. Vahabzadeh, and C. Caloz, Simultaneous control of the spatial and temporal spectra of light with space-time varying metasurfaces, IEEE Trans. Antennas Propag. **67,** 2430 (2019).

[34] A. M. Shaltout, V. M. Shalaev, and M. L. Brongersma, Spatiotemporal light control with active metasurfaces, Science **364,** eaat3100 (2019).

[35] D. Ramaccia, D. L. Sounas, A. Alù, A. Toscano, and F. Bilotti, Phase-induced frequency conversion and doppler effect with time-modulated metasurfaces, IEEE Trans. Antennas Propag. **68,** 1607 (2019).

[36] See Supplemental Material at http://link.aps.org/supplemental/10.1103/PhysRevLett.128.244301 for more details on definitions of system parameters, experimental setup and procedures, tunability of the linear active meta-layer, and simulations of metasurfaces.

[37] A. M. Shaltout, K. G. Lagoudakis, J. van de Groep, S. J. Kim, J. Vučković, V. M. Shalaev, and M. L. Brongersma, Spatiotemporal light control with frequency-gradient metasurfaces, Science **365,** 374 (2019).